ISSN 1067-8212, Russian Journal of Non-Ferrous Metals, 2025, Vol. 66, No. 1, pp. 35–46. © Pleiades Publishing, Ltd., 2025.

Tailoring of Smart Nanocomposites of ZnO–ZnS as Balanced Semiconductors with Potent Adsorption in Advanced Facile Batteries

Fatemeh Mollaamin[a], * and Majid Monajjemi[b]

[a] *Department of Biomedical Engineering, Faculty of Engineering and Architecture, Kastamonu University, Kastamonu, Turkey*

[b] *Department of Chemical Engineering, Central Tehran Branch, Islamic Azad University, Tehran, Iran*

**e-mail: fmollaamin@kastamonu.edu.tr*

Received March 27, 2025; revised April 13, 2025; accepted May 16, 2025

Abstract—We employ first-principles calculations to investigate the structural stability and electronic properties of cubic zinc oxide (ZnO) and Zinc sulfide (ZnS) heteroclusters adsorbed with H_2O molecule. A comprehensive investigation on H_2O grabbing by ZnO/ZnS heteroclusters was carried out using DFT computations at the CAM–B3LYP–D3/6–311+G (d, p) level of theory. The notable fragile signal intensity close to the parallel edge of the nanocluster sample might be owing to H/OH binding induced non-spherical distribution of ZnO or ZnS heterocluster. The hypothesis of the energy adsorption phenomenon was confirmed by density distributions of CDD, TDOS and ESP for ZnO/ZnO–H_2O or ZnS/ZnS–H_2O. A vaster jointed area engaged by an isosurface map for H/OH adsorption on ZnO or ZnS surface towards formation of ZnO–H_2O or ZnS–H_2O complex due to labeling atoms of O1, Zn15, O27 or S27, H29, H30. Therefore, it can be considered that zinc in the functionalized ZnO or ZnS might have more impressive sensitivity for accepting the electrons in the process of H/OH adsorption. It is considerable that when all surface atoms of ZnO or ZnS are coated by OH and H groups, the semiconducting behavior is recovered. Our results open up the possibility of tailoring the electronic properties by controlling the surface adsorption sites.

Keywords: ZnO/ZnS heteroclusters, nanosensor, water adsorption, density functional theory

DOI: 10.1134/S1067821225600279

1. INTRODUCTION

Transparent, superhydrophilic materials are indispensable for their self-cleaning function, which has become an increasingly popular research topic, particularly in photovoltaic (PV) applications. It was reported hydrophilic and superhydrophilic ZnO by varying the morphology for use as a self-cleaning coating for PV applications [1–4].

The researchers have applied molecular dynamics simulations through a reactive force-field for ZnO–H_2O ambient. The force-field parameters were fitted to a dataset of energies, geometries and charges derived from density functional theory calculations [5–11]. The applied model has provided a good fit to the quantum mechanics reference data for the ZnO–H_2O system that was present in the dataset. The force-field has been used to study how H_2O is adsorbed, molecularly or dissociatively, at monolayer coverage on flat and stepped ZnO surfaces, at different temperatures. The results show that structures that promote hydrogen bonding are favored, and that the presence of steps promotes an increased level of hydroxylation in the water monolayers [12–15].

The cubic form of zinc sulfide (ZnS) is the prototype II–VI semiconductor with smallest lattice constant of $a_0 = 5.4102$ Å at 300 K and the primarily candidate for UV-light emitting devices because of its large band-gap energy around ~3.7 eV at room temperature [16–21].

Many research groups have attempted to dope anions and cations into the ZnO or ZnS lattice, which helps to reach various complex applications since its electronic structure and characteristics may be significantly adjusted [22–25]. The enhanced catalytic properties reveal the synergy between ZnO and ZnS functional nanomaterials, which upgrade the electron-hole pair, resulting in an enhanced catalytic performance under the visible region [26–29].

In this work, we analyzed the effect of H_2O adsorption on the properties of ZnO or ZnS heterocluster via the density of state, charge distribution, bond orders and HOMO–LUMO orbitals using DFT studies. The optimized ZnO or ZnS is shown in Figs. 1a and 1b, and the Zn and O or S atoms are also numbered to characterize the reaction pathway.

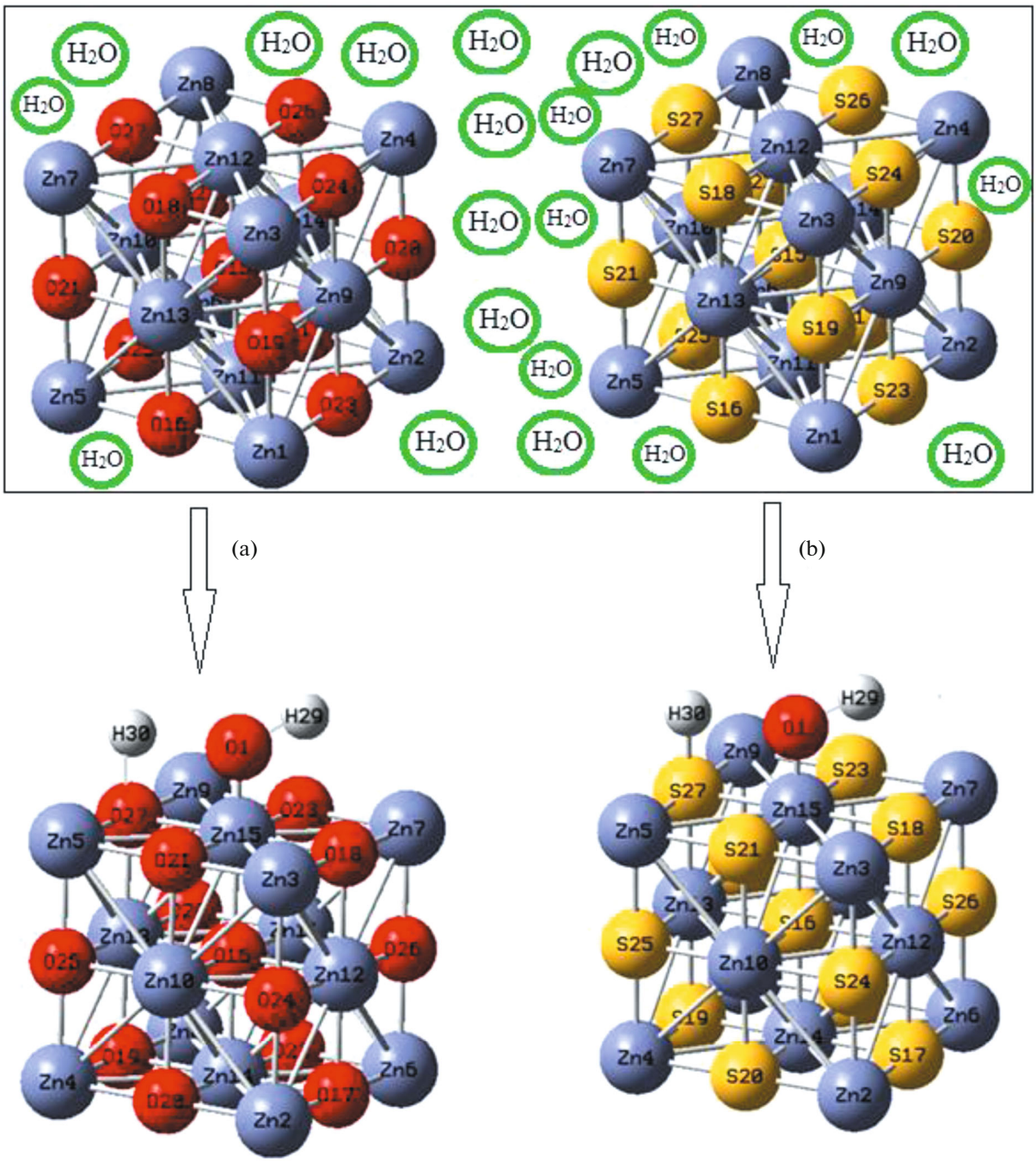

Fig. 1. Characterization of (a) ZnO/ZnO–H_2O and (b) ZnS/ZnS–H_2O heteroclusters through a labeled ring in clockwise manner including H, O, S, Zn towards H_2O-adsorption.

2. THEORY, MATERIALS AND COMPUTATION

The hydration of ZnO or ZnS and formation of ZnO–H_2O or ZnS–H_2O heterocluster [30–34] was calculated within the framework of first-principles calculation based on density functional theory (DFT) (Fig. 1). The rigid potential energy surface using density functional theory [35–48] was performed due to Gaussian 16 revision C.01 program package [49] and GaussView 6.1 [50]. The coordination input for energy storage on the solar cells has applied 6–311+G(d,p) and EPR-3 basis sets [51, 52].

First, we optimized the structural parameters of the nanocluster of ZnO or ZnS and hydrated nanocluster of ZnO–H_2O or ZnS–H_2O for obtaining the highest short-circuit current density. Figure 1 shows the process of H_2O-adsorption on nanocluster of ZnO

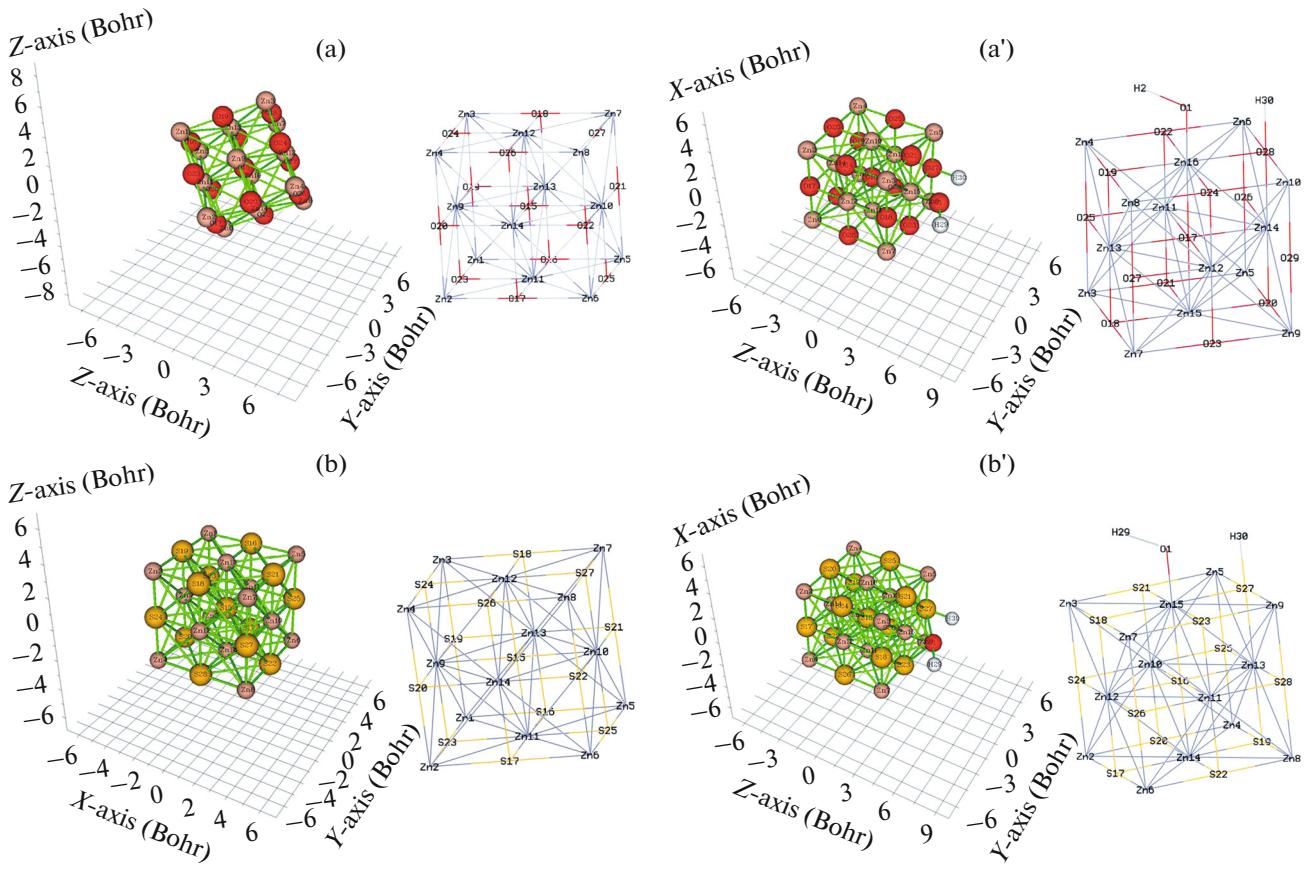

Fig. 2. CDD graphs for heteroclusters of (a) ZnO, (a') ZnO–H_2O, (b) ZnS, and (b') ZnS–H_2O.

or ZnS which is varied to maximize the absorption in the active region. This is a utility used to calculate ring area and perimeter, since ring area is sometimes involved in wavefunction analysis. In this function, it is needed to input the index of the atoms in the ring in clockwise manner which can conclude the total ring area and total ring perimeter for a tailored ring as 9.4242 and 12.2796 Å^2 for ZnO (Fig. 1a) and 9.4240 and 12.2794 Å^2 for ZnS, respectively (Fig. 1b).

3. RESULTS AND DISCUSSION

The applied model has provided a good fit to the quantum mechanics reference data for the ZnO–H_2O or ZnS–H_2O systems that was present in the dataset. The force-field has been used to study how water is adsorbed, molecularly at monolayer coverage on ZnO or ZnS surfaces. The amounts of charge density differences "CDD" [53] is measured by considering isolated atoms or non-interacting ones. The mentioned approximation can be the lightest to use because the superposition value may be received from the primary status of the self-consistency cycle in the code that carries out the density functional theory (Figs. 2a, 2a', 2b, 2b'). Figure 2a and 2b indicates all Zn, O or S atoms of ZnO or ZnS fluctuating around –9 to –1 Bohr. In Figs. 2a', 2b', the atom of Zn15, O27 or S27 from ZnO–H_2O or ZnS–H_2O and O1, H29, H30 from H_2O molecule accompanying other Zn, O or S atoms from ZnO–H_2O or ZnS–H_2O have shown the fluctuation around –1 to +1 Bohr and –9 to +1 Bohr, respectively.

Furthermore, atomic charge was discussed during H_2O adsorption by ZnO or ZnS towards formation of ZnO–H_2O or ZnS–H_2O. The atomic charge of Zn, O or S, and H/OH adsorbed on ZnO or ZnS have been measured. The values detect that with adding H_2O, the negative atomic charge of oxygen atoms of O16, O17, O18, O19, O20, O21, O22, O23, O24, O25, O26, O27, O28 in ZnO–H_2O has changed through coating of ZnO with H/OH. In fact, ZnO–H_2O has shown more efficiency than ZnO for admitting the electron from electron donor of O16 to O28 (Fig. 3a). However, the negative atomic charge of zinc atoms and loss of negative atomic charge of sulfur in ZnS/ZnS–H_2O have been observed through Fig. 3b. The changes of charge density analysis in the adsorption process have illustrated that ZnO and ZnO–H_2O nanoclusters have shown the "Bader charge" of –1.747 and –1.900 coulomb, respectively. The differences of charge density for these structures are measured as: $\Delta Q_{\text{ads. ZnO–H}_2\text{O}} =$ –0.153 coulomb. The changes of charge density anal-

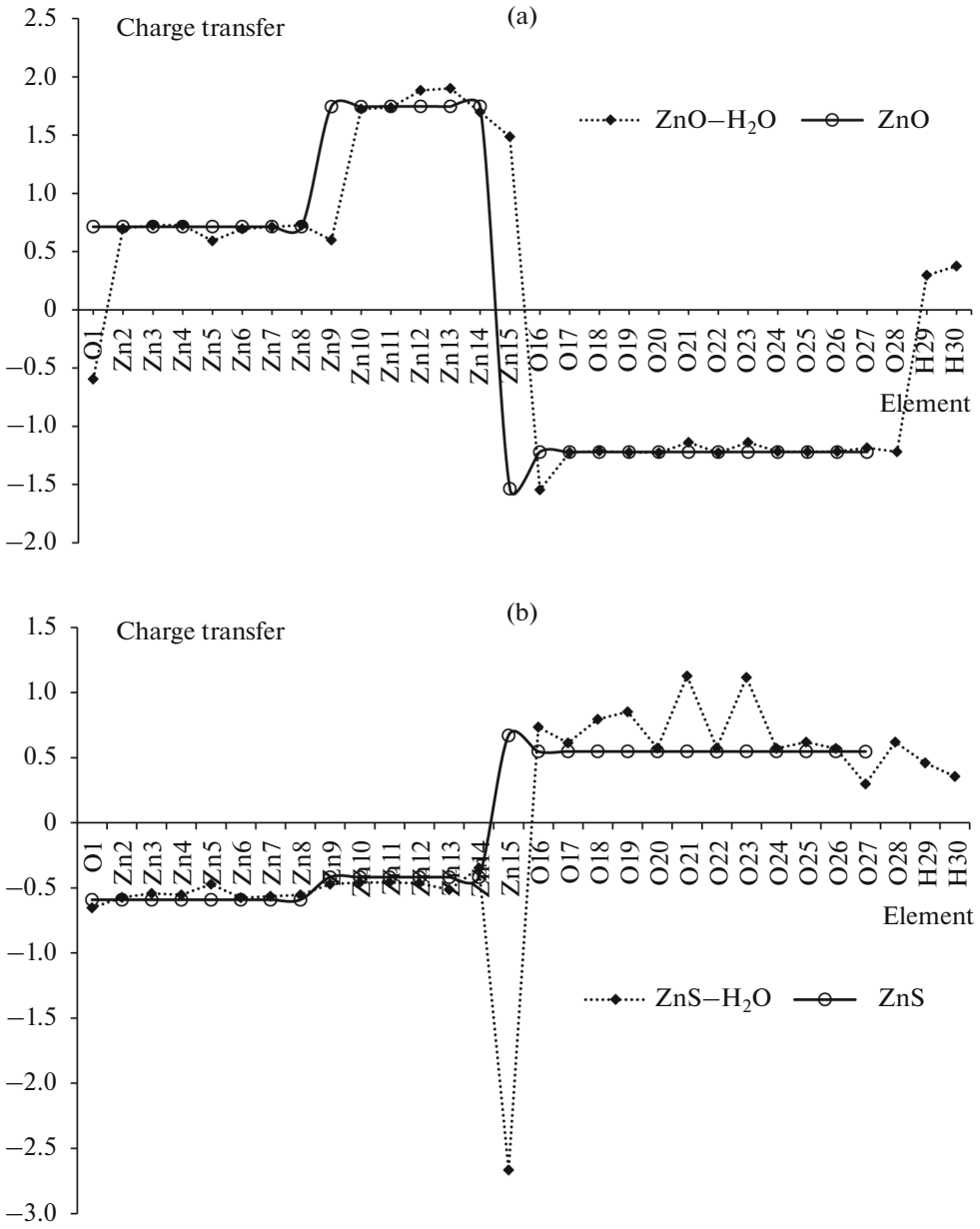

Fig. 3. The fluctuation of atomic charge (Q/coulomb) for (a) ZnO/ZnO–H_2O and (b) ZnS/ ZnS–H_2O.

ysis in the adsorption process have illustrated that ZnS and ZnS–H_2O nanoclusters have shown the "Bader charge" [54] of –0.670 and –2.667 coulomb, respectively. The differences of charge density for these structures are measured as: $\Delta Q_{\text{ads. ZnS–H}_2\text{O}} = -1.997$ coulomb.

To better understand the different adsorption characteristics of ZnO/ZnO–H_2O and ZnS/ZnS–H_2O heteroclusters, total density of states (TDOS) using Multiwfn program [55, 56] has been measured. This parameter can indicate the existence of important chemical interactions often on the convex side (Figs. 4a, 4a', 4b, 4b'). In an isolated system (such as molecule), the energy levels are discrete, the concept of density of state (DOS) is supposed to be completely valueless in this situation. Therefore, the original total DOS (TDOS) of the isolated system can be written as [57]:

$$\mathrm{TDOS}(E) = \sum_i \delta(E - \epsilon_i), \tag{1}$$

where ϵ_i is eigenvalue set of single-particle Hamilton, δ is Dirac delta function. If δ is replaced by broadening function $F(x)$, such as Gaussian, Lorentzian and pseudo-Voigt function, we get broadened TDOS. The normalized Gaussian function is described as:

$$G(x) = \frac{1}{c\sqrt{2\pi}} e^{-\frac{x^2}{2c^2}}, \quad \text{where} \quad c = \frac{\mathrm{FWHM}}{2\sqrt{2\ln x}}, \tag{2}$$

FWHM is acronmy of "full width at half maximum", it is an acceptable factor in Multiwfn. Moreover, the curve map of broadened partial DOS (PDOS) and overlap DOS (OPDOS) are valuable for visualizing orbital composition analysis, PDOS function of fragment A is defined as:

$$\mathrm{PDOS}_A(E) = \sum_i \Xi_{i,A} F(E - \epsilon_i), \quad (3)$$

where $\Xi_{i,A}$ is the composition of fragment A in orbital i. The OPDOS between fragment A and B is defined as:

$$\mathrm{OPDOS}_{A,B}(E) = \sum_i X^i_{A,B} F(E - \epsilon_i), \quad (4)$$

where $X^i_{A,B}$ is the composition of total cross term between fragment A and B in orbital i.

In the TDOS map, each discrete vertical line corresponds to a molecular orbital (MO), the dashed line highlights the position of HOMO. The curve is the TDOS simulated based on the distribution of MO energy levels. In the negative part, the region around −0.60 to −0.80 a.u. has obviously larger state density than other regions for ZnO and ZnO–H_2O nanoclusters (Figs. 4a, 4a'). However, it has been shown a larger state density through pointed peaks for ZnO–H_2O (Fig. 4a') than ZnO (Fig. 4a) around −0.20 to −0.40 a.u. It is remarkable that when all surface atoms of ZnO are coated by OH and H groups, the semiconducting behavior is recovered. Our results open up the possibility of tailoring the electronic properties by controlling the surface adsorption sites. In the positive part, the region around 0.1 to 0.2 a.u. has obviously larger state density than other regions for ZnS and ZnS–H_2O nanoclusters (Figs. 4b, 4b').

This function measures the electrostatic interaction between a unit point charge placed at **r** and the system of interest. A positive (negative) value implies that the current position is dominated by nuclear (electronic) charges. Molecular electrostatic potential (ESP) has been widely used for prediction of nucleophilic and electrophilic sites for a long time. It is also valuable in studying hydrogen bonds, halogen bonds, molecular recognitions and the intermolecular interaction of aromatics [58–60]. Notice that evaluating ESP is much more time-consuming than evaluating other functions. Also note that ESP in Multiwfn is evaluated exactly by nuclear attractive integrals rather than using approximate methods (such as multipole expansion, numerical Poisson equation), hence you may find the results generated by Multiwfn are somewhat different from those outputted by other quantum chemistry codes. In order to speed up ESP evaluation, Multiwfn ignores some integrals that have little contributions. The threshold for ignoring is controlled by "espprecutoff" in settings.ini, enlarging this parameter results in more accurate ESP value, but also brings more computational cost. The ESP evaluated under default value is accurate enough in general cases.

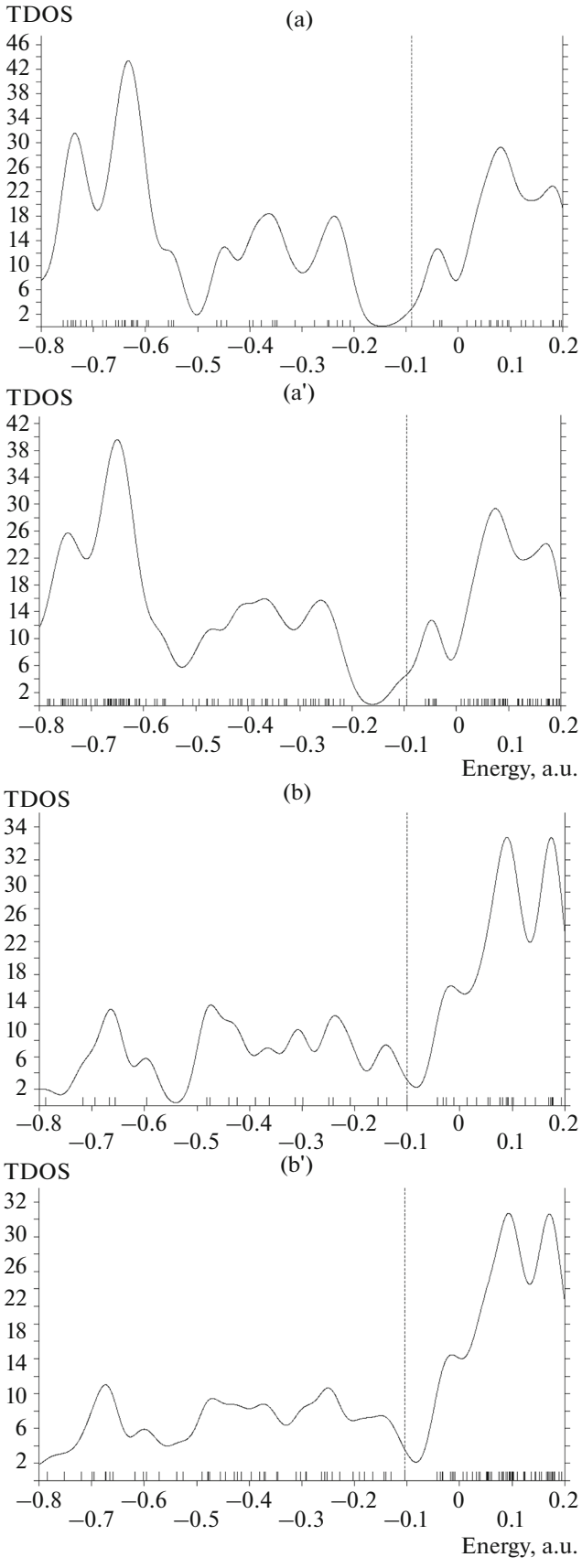

Fig. 4. TDOS graphs of heteroclusters of (a) ZnO, (a') ZnO–H_2O, (b) ZnS, and (b') ZnS–H_2O.

Table 1. LUMO, HOMO, and energy gap (ΔE) for ZnO and ZnS through H/OH adsorption and formation of ZnO–H_2O and ZnS–H_2O heteroclusters

Heteroclusters	E_{HOMO}, eV	E_{LUMO}, eV	$\Delta E = E_{LUMO} - E_{HOMO}$, eV
ZnO	−2.4280	−1.3056	1.1223
ZnO–H_2O	−2.6110	−1.6053	1.0056
ZnS	−2.7413	−1.1723	1.5690
ZnS–H_2O	−2.7459	−1.1762	1.6696

Table 2. The bond order of Mayer, Wiberg, Mulliken, Laplacian and Fuzzy from mixed alpha and beta density matrix for ZnO and ZnS through H/OH adsorption and formation of ZnO–H_2O and ZnS–H_2O heteroclusters

Bond order	ZnO–H_2O			ZnS–H_2O		
	O1–Zn15	O1–H29	O27–H30	O1–Zn15	O1–H29	S27–H30
Mayer	1.1308	0.6507	0.4783	1.2782	0.6905	0.8056
Wiberg	1.7176	0.6631	0.4490	1.0554	0.6397	0.6436
Mulliken	1.9120	0.1727	0.0573	1.8753	0.1573	0.1864
Laplacian	1.6451	0.2169	0.1505	1.7453	0.2014	0.2491
Fuzzy	1.6561	0.6878	0.4321	1.5246	0.6273	0.6852

The heteroclusters of ZnO/ZnO–H_2O and ZnS/ZnS–H_2O can be defined by ESP graphs owing to exploring their delocalization/localization characterizations of electrons and chemical bonds (Figs. 5a, 5a', 5b, 5b'). Covalent zones have high ESP value, the electron depletion zones between valence shell and inner shell are indicated by the blue circles around nuclei (Figs. 5a, 5a', 5b, 5b'). The counter map of ESP for ZnO/ZnO–H_2O (Figs. 5a, 5a') and ZnS/ZnS–H_2O (Figs. 5b, 5b') has shown the localized orbital locator through H/OH adsorption. ZnO–H_2O or ZnS–H_2O heterocluster indicates a larger isosurface map of the localized orbital locator due to labeling atoms of O1, Zn15, O27 or S27, H29, H30. A narrower connected area occupied by an isosurface map means that localized orbital locator is relatively difficult. However, the large counter map of ESP for ZnO–H_2O or ZnS–H_2O can confirm that ZnO or ZnS can be a promising semiconductor material for various applications.

Moreover, intermolecular orbital overlap integral is important in discussions of intermolecular charge transfer which can calculate HOMO-HOMO and LUMO-LUMO overlap integrals between the H/OH and heterocluster of ZnO or ZnS. The applied wavefunction level is CAM–B3LYP–D3/6–311+G(d,p) that correspond to HOMO and LUMO, respectively (Table 1).

Mulliken bond order with a small accord with empirical bond order is not appropriate for quantifying bonding strength, for which Mayer bond order always performs better [61, 62] (Table 2). The results have indicated Laplacian bond order [63] by a perpendicular cohesion with bond polarity, bond dissociation energy and bond vibrational frequency. Besides, measurement of "Fuzzy bond order" requests running Becke's density functional theory [64–70] of numerical integration [71].

4. CONCLUSIONS

Remarkable attention has recently been given to ZnO or ZnS as a promising multifunctional material with wide-ranging technological applications. Understanding the interaction of water with ZnO or ZnS is important for this material to be used in gas sensing, catalysis and biomedical applications. In summary, H_2O grabbing on the ZnO or ZnS was investigated by first-principles calculations. We have provided ZnO or ZnS heterocluster, then the geometrical parameters of H/OH adsorption on the surface of ZnO or ZnS through the absorption status and current charge density were studied. ZnO–H_2O or ZnS–H_2O heterocluster indicates a larger isosurface map of electron delocalization due to labeling atoms of O1, Zn15, O27 or S27, H29, H30. A narrower connected area occupied by an isosurface map means that electron delocalization is relatively difficult. However, the large

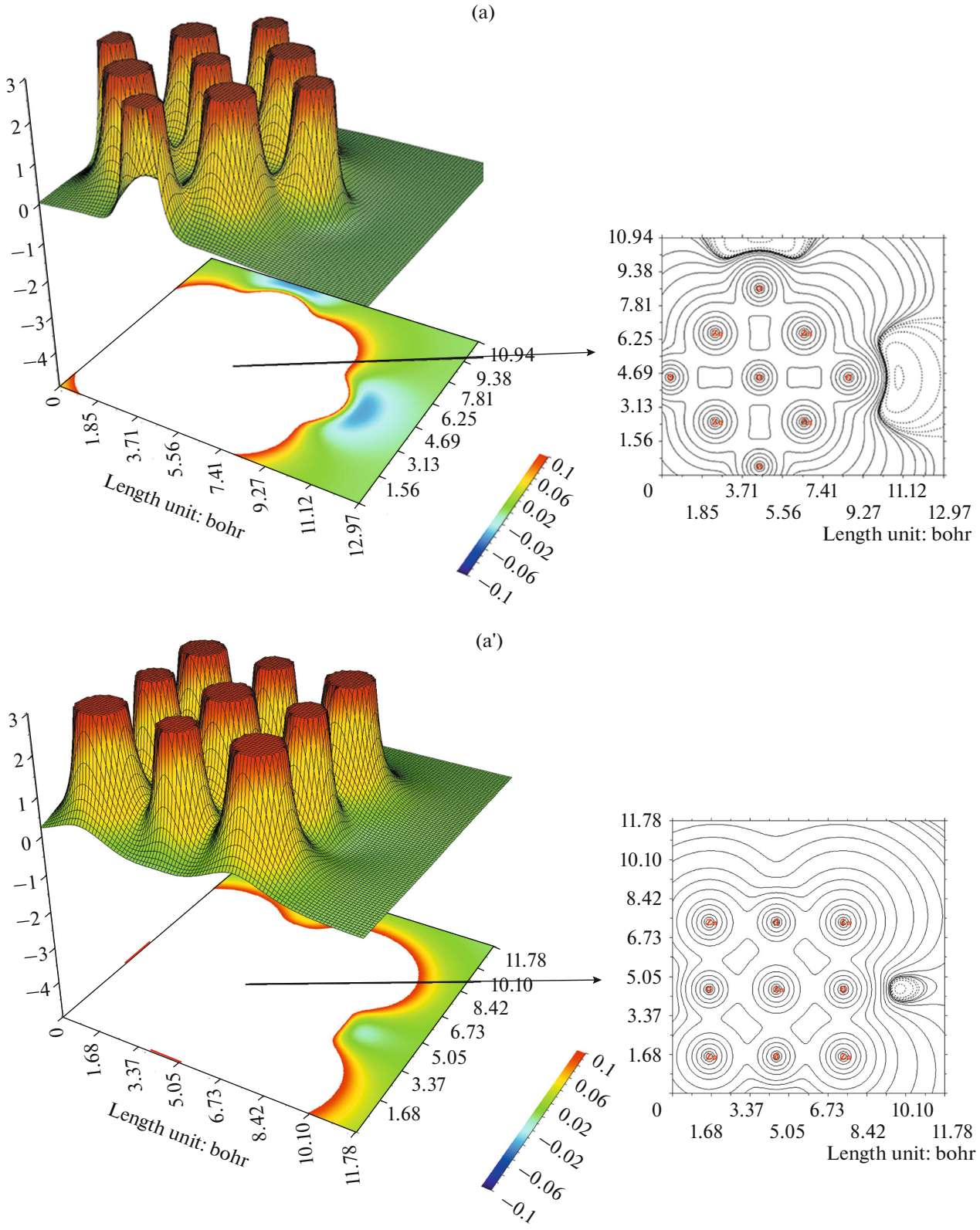

Fig. 5. The graphs of ESP for heteroclusters of (a) ZnO, (a') ZnO–H_2O, (b) ZnS, and (b') ZnS–H_2O (Counter line map on the right and shaded surface map with projection in the left).

(b)

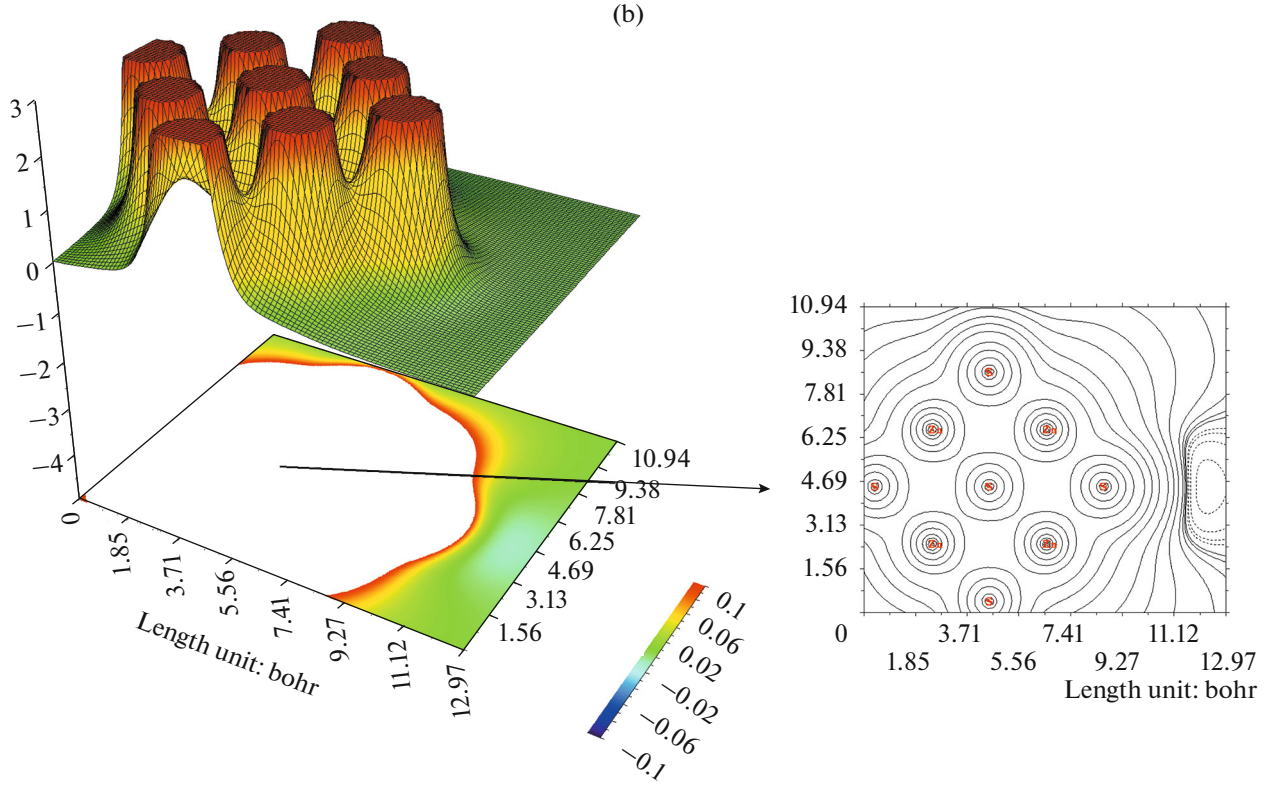

(b')

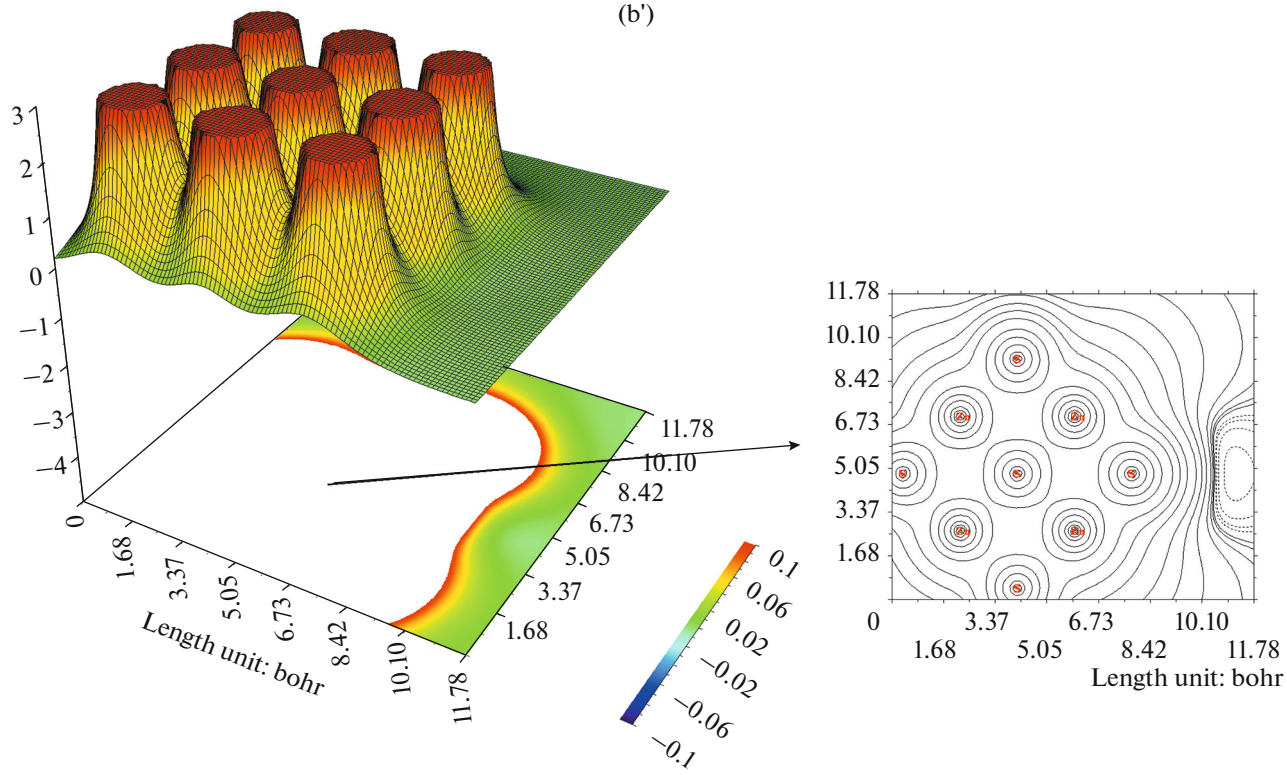

Fig. 5. (Contd.)

counter map of ESP for ZnO–H_2O or ZnS–H_2O can confirm that ZnO or ZnS can be a promising semiconductor material for various applications.

ACKNOWLEDGMENTS

In successfully completing this paper and its research, the authors are grateful to Kastamonu University.

FUNDING

This work was supported by ongoing institutional funding. No additional grants to carry out or direct this particular research were obtained.

CONFLICT OF INTEREST

The authors of this work declare that they have no conflicts of interest.

REFERENCES

1. Abbasov, I.I., Musayev, M.A., Huseynov, C.I., Eyyubov, Q.Y., Hasimova, et al., A study of impurity defect photoluminescence in ZnSe:Cr and ZnSe:Fe in the near infrared at room temperature, *Adv. Phys. Res.,* 2023, vol. 5, no. 3, pp. 192–199.
2. Zhang, X.Q. and Zhang, B., Effect of pressure on the structural, mechanical, and electronic properties of monoclinic $ZnWO_4$, *Russ. J. Phys. Chem. B,* 2023, vol. 17, no. 5, pp. 1049–1056. https://doi.org/10.1134/S1990793123050135
3. Ikim, M.I., Spiridonova, E.Yu., Gromov, V.F., et al., effect of the formation method of ZnO–In_2O_3 composites on their structural characteristics and conductivity, *Russ. J. Phys. Chem. B.,* 2024, vol. 18, pp. 283–288. https://doi.org/10.1134/S199079312401010X
4. Zverev, A.S., Zvekov, A.A., Pugachev, V.M., et al., Controlling the sensitivity of pentaerythritol tetranitrate to visible laser radiation by the addition of ZnO: Ag nano-powder, *Russ. J. Phys. Chem. B,* 2023, vol. 17, no. 5, pp. 1135–1142. https://doi.org/10.1134/S1990793123050147
5. Yuan, X., Tan, X., and Liu, B., Structural, mechanical, electronic and optical properties of spinel $ZnAl_2O_4$ underpressure from first-principles calculations, *Russ. J. Phys. Chem. B,* 2023, vol. 17, no. 4, pp. 886–895. https://doi.org/10.1134/S1990793123040322
6. Ankam, V., Karka, G., and Reddy, L.G., Structural and optical properties of copper-doped zinc ferrites using solid state reaction method, *Mater. Int.,* 2025, vol. 7, no. 1, p. 1. https://doi.org/10.33263/Materials71.001
7. Parmonov, S., Sharipov, K., Mirzavaliyev, D., Makhmudova, F., Askarova, N., Toshkodirova, R., Abdullaeva, N., Rifky, M., Harris, J.M., and Kambarov, A., The technology of obtaining powders used in the production of solid alloys, *New Mater., Compd. Appl.,* 2024, vol. 8, no. 3, pp. 450–458. https://doi.org/10.62476/nmca83450
8. Kirana, P., Prashantkumar, C.S., Soundarya, R., Shwetha, G.S., Kalasad, M.N., and Gayathri, D., Tinospora cordifolia's green synthesis approach: comparative study on biogenic and chemical synthesis of zinc oxide and zinc sulfide nanoparticles, *Mater. Int.,* 2024, vol. 6, no. 4, p. 40. https://doi.org/10.33263/Materials64.040
9. Olkhovskaya, I.P., Krokhmal, I.I., and Glushchenko, N.N., Improvement of the morphophysiological parameters of pepper after the presowing treatment of seeds with zinc nanoparticles, *Russ. J. Phys. Chem. B,* 2024, vol. 18, pp. 527–532. https://doi.org/10.1134/S1990793124020295
10. Bhat, M., Sekhar, E.V., and Sagar, B.K., Synthesis, characterization, and photocatalytic applications of ZnO–Fe_2O_3/PVA nanocomposite, *Letters in Applied NanoBioScience,* 2025, vol. 14, no. 1, p. 45. https://doi.org/10.33263/LIANBS141.045
11. Kumar, N., Sharma, R., Aggarwal, N.K., and Singh, A.P., Utilization of Parthenium hysterophorus for the synthesis of lignin-ZnO nanocomposites aimed at boosting antibacterial and antioxidant activity, *Letters in Applied NanoBioScience,* 2024, vol. 13, no. 4, p. 171. https://doi.org/10.33263/LIANBS134.171
12. Xiong, H.M., Liu, D.P., Xia, Y.Y., and Chen, J.S., Polyether-grafted ZnO nanoparticles with tunable and stable photoluminescence at room temperature, *Chem. Mater.,* 2005, vol. 17, no. 12, pp. 3062–3064. https://doi.org/10.1021/cm050556r
13. Agarwal, D.C., Singh, U.B., Gupta, S., Singhal, R., Kulriya, P.K., Singh, F., Tripathi, A., Singh, J., Joshi, U.S., and Avasthi, D.K., Enhanced room temperature ferromagnetism and green photoluminescence in Cu doped ZnO thin film synthesized by neutral beam sputtering, *Sci. Rep.,* 2019, vol. 9, p. 6675. https://doi.org/10.1038/s41598-019-43184-9
14. Wolska, E., Kaszewski, J., Kiełbik, P., Grzyb, J., Godlewski, M.M., and Godlewski, M., Rare earth activated ZnO nanoparticles as biomarkers, *Opt. Mater.,* 2014, vol. 36, no. 10, pp. 1655–1659. https://doi.org/10.1016/j.optmat.2013.12.032
15. Lim, J.H., Kang, C.K., Kim, K.K., Park, I.K., Hwang, D.K., and Park, S.J., UV electroluminescence emission from ZnO light-emitting diodes grown by high-temperature radiofrequency sputtering, *Adv. Mater.,* 2006, vol. 18, no.20, pp. 2720–2724. https://doi.org/10.1002/adma.200502633
16. Tolubayeva, D.B., Gritsenko, L.V., Kedruk, Y.Y., Aitzhanov, M.B., Nemkayeva, R.R., and Abdullin, K.A., Effect of hydrogen plasma treatment on the sensitivity of ZnO based electrochemical non-enzymatic biosensor, *Biosensors,* 2023, vol. 13, no. 8, p. 793. https://doi.org/10.3390/bios13080793
17. Liu, H., Zhang, Y., Zhang, H., Wang, L., Wang, T., Han, Z., Wu, L., and Liu, G., Effect of plasma vitamin C levels on Parkinson's disease and age at onset: A Mendelian randomization study, *J. Transl. Med.,* 2021, vol. 19, no. 1, p. 221. https://doi.org/10.1186/s12967-021-02892-5
18. Hegde, V.N., Biomedical applications of ZnO nanoparticles: a paradigm shift in healthcare, *Letters in Applied NanoBioScience,* 2024, vol. 13, no. 3, p. 132. https://doi.org/10.33263/LIANBS133.132

19. Chang, S.-C., Hu, J.-C., Chan, H.-T., and Hsiao, C.-A., Influence of processing time in hydrogen plasma to prepare gallium and aluminum codoped zinc oxide films for low-emissivity glass, *Coatings,* 2022, vol. 12, no. 7, p. 945. https://doi.org/10.3390/coatings12070945

20. Chang, S.-C., Li, T.-H., and Chan, H.-T., Hydrogen plasma annealed titanium dioxide oxide/aluminum-doped zinc oxide films applied in low emissivity glass, *Int. J. Electrochem. Sci.,* 2021, vol. 16, no. 8, p. 210817. https://doi.org/10.20964/2021.08.34

21. Zhang, C., Cao, Z., Zhang, G., Yan, Y., Yang, X., Chang, J., Song, Y., Jia, Y., Pan, P., Mi, W., et al., An electrochemical sensor based on plasma-treated zinc oxide nanoflowers for the simultaneous detection of dopamine and diclofenac sodium, *Microchem. J.,* 2020, vol. 158, p. 105237. https://doi.org/10.1016/j.microc.2020.105237

22. Nundy, S., Ghosh, A., and Mallick, T.K., Hydrophilic and super-hydrophilic self-cleaning coatings by morphologically varying ZnO microstructures for photovoltaic and glazing applications, *ACS Omega,* 2020, vol. 5, no. 2, pp. 1033–1039. https://doi.org/10.1021/acsomega.9b02758

23. Yakovenko, I.S. and Kiverin, A.D., Influence of water microdroplets on the development of hydrogen-air flame instability in a channel, *Russ. J. Phys. Chem. B,* 2024, vol. 18, pp. 1069–1076. https://doi.org/10.1134/S1990793124700623

24. Monajjemi, M., Mohammadi, S., Shahriari, S., and Mollaamin, F., Experimental and theoretical studies of ZnO nanotubes: an approach to chemical physics characterization of ZnONTs, including morphology, piezoelectric, and density of states, *Russ. J. Phys. Chem. B,* 2024, vol. 18, no. 1, pp. 308–324. https://doi.org/10.1134/S1990793124010342

25. Zainabidinov, S.Z., Boboev, A.Y., Rasulova, M.B., and Yunusaliyev, N.Y., X-ray diffraction analysis, optical characteristics and electro-physical properties of the NZnO/P–NiO structure grown by the spray pyrolysis method, *New Mater., Compd. Appl.,* 2024, vol. 8, no. 3, pp. 411–421. https://doi.org/10.62476/nmca83411

26. Yakush, E.A., Kim, A.V., and Medvedev, N.N., Investigation of the behavior of dioxadet molecules in water by molecular dynamics simulation, *Russ. J. Phys. Chem. B,* 2024, vol. 18, pp. 252–257. https://doi.org/10.1134/S199079312401038X

27. Vasin, A.A., Dobryakov, A.L., and Kochev, S.Y., et al., Relaxation of multiple excitons in ZnCdS and ZnCdS/ZnS alloy quantum dots, *Russ. J. Phys. Chem. B,* 2024, vol. 18, pp. 1646–1650. https://doi.org/10.1134/S1990793124701380

28. Castro, A., Calderon, S., and Marques, L., Oxygen adsorption on polar and non-polar Zn:ZnO heterostructures from first principles, *Materials,* 2023, vol. 16, no. 3, p. 1275. https://doi.org/10.3390/ma16031275

29. Wang, G., Huang, B., Li, Z., Lou, Z., Wang, Z., Dai, Y., and Whangbo, M.-H., Synthesis and characterization of ZnS with controlled amount of S vacancies for photocatalytic H_2 production under visible light, *Sci. Rep.,* 2015, vol. 5, no. 1, p. 8544. https://doi.org/10.1038/srep08544

30. Khan, A.U., Tahir, K., Albalawi, K., et al., Synthesis of ZnO and ZnS nanoparticles and their structural, optical, and photocatalytic properties synthesized via the wet chemical method, *Mater. Chem. Phys.,* 2022, vol. 291, p. 126667. https://doi.org/10.1016/j.matchemphys.2022.126667

31. Zagorac, D., Zagorac, J., Pejić, M., Matović, B., and Schön, J.C., Band gap engineering of newly discovered ZnO/ZnS polytypic nanomaterials, *Nanomaterials,* 2022, vol. 12, no. 9, p. 1595. https://doi.org/10.3390/nano12091595

32. De Moraes, N.P., Marins, L.G.P., De Moura Yamanaka, M.Y., Bacani, R., da Silva Rocha, R., and Rodrigues, L.A., Efficient photodegradation of 4-chlorophenol under solar radiation using a new ZnO/ZnS/carbon xerogel composite as a photocatalyst, *J. Photochem. Photobiol., A,* 2021, vol. 418, p. 113377. https://doi.org/10.1016/j.jphotochem.2021.113377

33. Bolatov, A., Manjovelo, A., Chouchene, B., Balan, L., Gries, T., Medjahdi G., Uralbekov, B., and Schneider, R., Ternary ZnS/ZnO/graphitic carbon nitride heterojunction for photocatalytic hydrogen production, *Materials,* 2024, vol. 17, no. 19, p. 4877. https://doi.org/10.3390/ma17194877

34. Chaudhari, V., Dharmadhikari, M., and Kolhe, V., Experimental analysis of thermal performance for heat pipe heat exchanger with ZnO nanofluid, *Letters in Applied NanoBioScience,* 2024, vol. 13, no. 2, p. 80. https://doi.org/10.33263/LIANBS132.080

35. Mollaamin, F. and Monajjemi, M., Designing novel nanomaterials for Li-ion batteries: A physico-chemical study through hydrogen-powered horizons, *New Mater., Compd. Appl.,* 2024, vol. 8, no. 3, pp. 303–323. https://doi.org/10.62476/nmca83303

36. Xin, Z., He, Q., Wang, S., et al., Recent progress in ZnO-based nanostructures for photocatalytic antimicrobial in water treatment: a review, *Appl. Sci.,* 2022, vol. 12, no. 15, p. 7910. https://doi.org/10.3390/app12157910

37. Mollaamin, F., Shahriari, S., Monajjemi, M., and Khalaj, Z., Nanocluster of aluminum lattice via organic inhibitors coating: a study of freundlich adsorption, *J. Cluster Sci.,* 2023, vol. 34, no. 3, pp. 1547–1562. https://doi.org/10.1007/s10876-022-02335-1

38. Pedra, T.K., Carvalho, R.D., Fernandes, C.D., et al., Physical and chemical approaches of photovoltaic parameters in dye-sensitized solar cells to ZnO/ZnS:rGO-based photoelectrodes, *Appl. Sci.,* 2025, vol. 15, no. 1, p. 291. https://doi.org/10.3390/app15010291

39. Mollaamin, F. and Monajjemi, M., Transition metal (X = Mn, Fe, Co, Ni, Cu, Zn)-doped graphene as gas sensor for CO_2 and NO_2 detection: A molecular modeling framework by DFT perspective, *J. Mol. Model.,* 2023, vol. 29, no. 4, p. 119. https://doi.org/10.1007/s00894-023-05526-3

40. Mollaamin, F. and Monajjemi, M., Selectivity and sensitivity evaluation of embedded BN-nanostructure as a gas detector for air pollution scavenging: a theoretical study,

Russ. J. Phys. Chem. B, 2024, vol. 18, pp. 1177–1198. https://doi.org/10.1134/S1990793124700507

41. Mollaamin, F. and Monajjemi, M., Tailoring and functionalizing the graphitic-like GaN and GaP nanostructures as selective sensors for NO, NO_2, and NH_3 adsorbing: a DFT study, *J. Mol. Model.,* 2023, vol. 29, p. 170. https://doi.org/10.1007/s00894-023-05567-8
42. Jin, X., Chen, J., Chen, F., et al., Solid-state synthesis of ZnO/ZnS photocatalyst with efficient organic pollutant degradation performance, *Catalysts,* 2022, vol. 12, no. 9, p. 981. https://doi.org/10.3390/catal12090981
43. Mollaamin, F. and Monajjemi, M., In Silico-DFT Investigation of nanocluster alloys of Al–(Mg,Ge,Sn) coated by nitrogen heterocyclic carbenes as corrosion inhibitors, *J. Cluster Sci.,* 2023, vol. 34, no. 6, pp. 2901–2918. https://doi.org/10.1007/s10876-023-02436-5
44. Isac, L. and Enesca, A., Recent developments in ZnS-based nanostructures photocatalysts for wastewater treatment, *Int. J. Mol. Sci.,* 2022, vol. 23, no. 24, p. 15668. https://doi.org/10.3390/ijms232415668
45. Mollaamin, F. and Monajjemi, M., Doping of graphene nanostructure with iron, nickel and zinc as selective detector for the toxic gas removal: a density functional theory study, *C–J. Carbon Res.,* 2023, vol. 9, no. 1, p. 20. https://doi.org/10.3390/c9010020
46. Mollaamin, F. and Monajjemi, M., Adsorption ability of Ga_5N_{10} nanomaterial for removing metal ions contamination from drinking water by DFT, *Int. J. Quantum. Chem.,* 2024, vol. 124, no. 2, p. e27348. https://doi.org/10.1002/qua.27348
47. Mollaamin, F. and Monajjemi, M., Molecular modelling framework of metal-organic clusters for conserving surfaces: Langmuir sorption through the TD-DFT/ONIOM approach, *Mol. Simul.,* 2022, vol. 49, no. 4, pp. 365–376. https://doi.org/10.1080/08927022.2022.2159996
48. Poliukhova, V., Lei, W., Khan, S., et al., ZnO/ZnS-polyvinyl alcohol hydrogel for photocatalytic H_2-Generation, *Catalysts,* 2022, vol. 12, no. 3, p. 272. https://doi.org/10.3390/catal12030272
49. Frisch M.J., Trucks G.W., Schlegel, H.B., Scuseria, G.E., Robb, M.A., et al., *Gaussian 16, Revision C.01,* Wallingford CT: Gaussian Inc., 2016.
50. Dennington, R., Keith, T.A., and Millam, J.M., *GaussView, Ver. 6.06.16,* Shawnee Mission, KS: Semichem Inc., 2016.
51. Yanai, T., Tew, D.P., and Handy, N.C., A new hybrid exchange–correlation functional using the Coulomb-attenuating method (CAM-B3LYP), *Chem. Phys. Lett.,* 2004, vol. 393, nos. 1–3, pp. 51–57. https://doi.org/10.1016/j.cplett.2004.06.011
52. Grimme, S., Ehrlich, S., and Goerigk, L., Effect of the damping function in dispersion corrected density functional theory, *J. Comput. Chem.,* 2011, vol. 32, no. 7, pp. 1456–1465. https://doi.org/10.1002/jcc.21759
53. Xu, Z., Qin, C., Yu, Y., Jiang, G., and Zhao, L., First-principles study of adsorption, dissociation, and diffusion of hydrogen on α-U (110) surface, *AIP Adv.,* 2024, vol. 14, no. 5, p. 055114. https://doi.org/10.1063/5.0208082
54. Mollaamin, F. and Monajjemi, M., Application of nanoscale boron nitride for encapsulation of noxious transition metals (Cr, Mn, Fe, Zn, W, Cd) in soil: physico-chemical characterization using DFT modeling, *Adv. Phys. Res.,* 2025, vol. 7, no. 1, pp. 5–28. https://doi.org/10.62476/apr.7105
55. Lu, T. and Chen, F., Multiwfn: A multifunctional wavefunction analyzer, *J. Comput. Chem.,* 2012, vol. 33, no. 5, pp. 580–592. https://doi.org/10.1002/jcc.22885
56. Lu, T., A comprehensive electron wavefunction analysis toolbox for chemists, Multiwfn, *J. Chem. Phys.,* 2024, vol. 161, p. 082503. https://doi.org/10.1063/5.0216272
57. Davtyan, A.H., Manukyan, Z.O., Arsentev, S.D., et al., Investigation of potential energy surfaces of reaction systems containing ethylene, hydrogen, and oxygen atoms by quantum chemical calculations, *Russ. J. Phys. Chem. B,* 2023, vol. 17, pp. 336–345. https://doi.org/10.1134/S1990793123020239
58. Murray, J.S. and Politzer, P., The electrostatic potential: an overview, *WIREs Comput. Mol. Sci.,* 2011, vol. 1, no. 2, pp. 153–163. https://doi.org/10.1002/wcms.19
59. Lopez, R., Martinez, F., Ema, I., et al., Efficient evaluation of molecular electrostatic potential in large systems, *Computation,* 2019, vol. 7, no. 4, p. 64. https://doi.org/10.3390/computation7040064
60. Murray, J.S., Riley, K.E., and Brinck, T., A Revival of molecular surface electrostatic potential statistical quantities: ionic solids and liquids, *Crystals,* 2024, vol. 14, no. 11, p. 995. https://doi.org/10.3390/cryst14110995
61. Mayer, I., Improved definition of bond orders for correlated wave functions, *Chem. Phys. Lett.,* 2012, vol. 544, pp. 83–86. https://doi.org/10.1016/j.cplett.2012.07.0
62. Mollaamin, F. and Monajjemi, M., Perspective of clean energy-saving by semiconducting quantum dot nanomaterials through photoelectric and density of states analysis, *J. Fluoresc.,* 2025. https://doi.org/10.1007/s10895-025-04207-z
63. Lu, T. and Chen, F., Bond order analysis based on the laplacian of electron density in fuzzy overlap space, *J. Phys. Chem. A.,* 2013, vol. 117, no. 14, pp. 3100–3108. https://doi.org/10.1021/jp4010345
64. Orel, V.B. and Manzhueva, A.A., Mechanism of one-pot stereoselective assembly of spiroketal derivatives from cyclohexanone and phenylacetylene in KOH/DMSO: a quantum chemical study, *Russ. J. Phys. Chem. B,* 2023, vol. 17, pp. 835–844. https://doi.org/10.1134/S1990793123040152
65. Touhami, H., Almi, K., Lakel, S., et al., Alkali doping nickel oxide thin films using sol-gel spin coated and density functional theory: structural and physical properties, *Russ. J. Phys. Chem. B,* 2023, vol. 17, no. 5,

pp. 1057–1068.
https://doi.org/10.1134/S1990793123050287

66. Mollaamin, F., Mohammadi, S., Khalaj, Z., et al., Computational modelling of boron nitride nanosheet for detecting and trapping of water contaminant, *Russ. J. Phys. Chem. B,* 2024, vol. 18, pp. 67–82. https://doi.org/10.1134/S1990793124010330
67. Makhaev, V.D., Petrova, L.A., Shilov, G.V., et al., The Structure of tetranuclear zirconium pivalate $Zr_4O_2[(CH_3)_3CCO_2]_{12}$ according to X-Ray diffraction analysis and quantum chemical calculations, *Russ. J. Phys. Chem. B,* 2024, vol. 18, pp. 388–397. https://doi.org/10.1134/S1990793124020258
68. Dyakov, Y.A., Adamson, S.O., Butkovskaya, N.I., et al., Collisional-induced chemical reactions between methane and criegee intermediates CH_2OO, CH_3CHOO, and $(CH_3)_2COO$: theoretical study, *Russ. J. Phys. Chem. B,* 2024, vol. 18, pp. 682–691. https://doi.org/10.1134/S1990793124700179
69. Zobov, V.E. and Lundin, A.A., On the statistical theory of the shape of multiple quantum NMR spectra in solids, *Russ. J. Phys. Chem. B,* 2024, vol. 18, pp. 1249–1262. https://doi.org/10.1134/S1990793124701070
70. Diniakhmetova, D.R. and Kolesov, S.V., Quantum-chemical simulation of the interaction of C_{60} fullerenes with growth radicals of the allyl chloride vinyl-type model, *Russ. J. Phys. Chem. B,* 2024, vol. 18, pp. 1478–1485. https://doi.org/10.1134/S1990793124701410
71. Wang, X., Zhang, X., Pedrycz, W., Yang, S.-H., and Boutat, D., Consensus of T-S fuzzy fractional-order, singular perturbation, multi-agent systems, *Fractal and Fractional,* 2024, vol. 8, no. 9, p. 523. https://doi.org/10.3390/fractalfract8090523

Publisher's Note. Pleiades Publishing remains neutral with regard to jurisdictional claims in published maps and institutional affiliations.
AI tools may have been used in the translation or editing of this article.